RESEARCH ARTICLE SUMMARY

NEUROSCIENCE

Ultrapotent chemogenetics for research and potential clinical applications

Christopher J. Magnus*, Peter H. Lee*, Jordi Bonaventura, Roland Zemla, Juan L. Gomez, Melissa H. Ramirez, Xing Hu, Adriana Galvan, Jayeeta Basu, Michael Michaelides, Scott M. Sternson†

INTRODUCTION: Localized control of neuron activity is important for both brain research and therapy. Chemogenetics is a method to control cellular activity by targeting defined cell populations with an exogenous receptor that is engineered to respond selectively to a small-molecule agonist. The approach is generalizable because a receptor-agonist combination can be used to activate or inhibit different neural populations in any brain region. Moreover, using agonists that are selective for the chemogenetic receptor allows cell type–specific modulation, in contrast to traditional pharmacology. Chemogenetic tools have achieved widespread utility in animal models, and there is growing interest in developing chemogenetic systems that are suitable for human therapeutic applications.

RATIONALE: Optimally, a chemogenetic system should have several characteristics for use in the nervous system: (i) The introduced receptor should be activated by low agonist doses; (ii) human use would be facilitated by a chemogenetic agonist that is already a safe and well-tolerated clinically approved drug that crosses the blood-brain barrier, whereas for research applications the agonist should be highly selective for the chemogenetic receptor over endogenous targets; (iii) chemogenetic receptors should be inert in the absence of the drug, lacking constitutive activity or responsiveness to endogenous ligands; (iv) the receptors should activate or inhibit neurons efficaciously, durably, and reversibly; and (v) the site and level of expression of the chemogenetic receptor should be measurable noninvasively. Existing chemogenetic systems did not fulfill all these criteria.

RESULTS: We identified mutations of the ligand-binding domain of the α7 nicotinic acetylcholine receptor that conferred potent activity to the FDA-approved smoking cessation drug varenicline. We created chimeric ligand-gated ion channels by combining these modified ligand-binding domains with ion pore domains from either the glycine receptor or the serotonin 3 receptor, which conduct chloride or cations, respectively. These two types of chemogenetic channels inhibit or activate neurons upon binding varenicline at concentrations below those used clinically to treat nicotine addiction. Varenicline is especially attractive for potential therapeutic applications because it shows limited metabolism, durable pharmacokinetics, and high oral and brain bioavailability. Chemogenetic inhibition or activation was sustained for at least 2 to 3 weeks of continual exposure to varenicline, indicating suitability for chronic use. Expression of the chemogenetic ion channels was visualized in animals by positron emission tomography, enabling noninvasive measurement of the expression and anatomic site of chemogenetic receptors. We showed robust responses to chemogenetic silencing of neurons using low doses of varenicline in mice and one monkey. Finally, we synthesized brain-penetrant analogs of varenicline with subnanomolar potency and with greatly enhanced selectivity for the chemogenetic receptors that were effective for modulation of neural activity in mice.

ON OUR WEBSITE

Read the full article at http://dx.doi.org/10.1126/science.aav5282

CONCLUSION: We developed a toolbox of modular ion channels and selective, ultrapotent agonists that can be used for targeted control of brain activity in rodent and primate models. Additional studies will be needed to establish long-term safety and efficacy with chemogenetic receptors for therapeutic applications, but this is facilitated by using varenicline. These chemogenetic technologies can advance research into neural circuit disorders while enabling extension to human therapies. ■

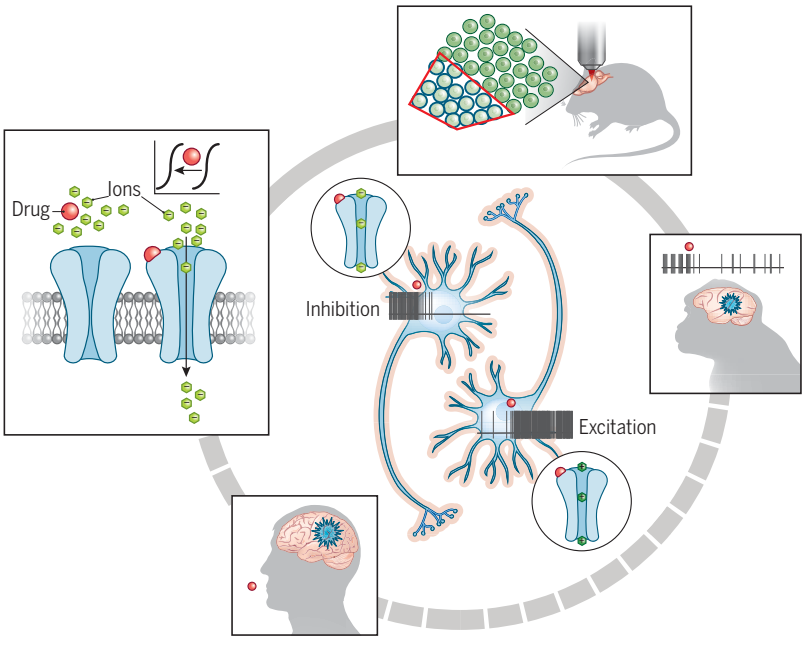

Chemogenetics for mice, monkeys, and potential therapy in humans. Modular ion channels were engineered to be activated by ultrapotent agonists, which selectively inhibit or excite activity in neurons expressing the chemogenetic receptors (blue). Neuron modulation was characterized by calcium imaging, electrophysiology, and behavior in mice and a monkey. These chemogenetic receptors and their FDA-approved agonists may facilitate translation of chemogenetics to therapies for human neurological diseases.

The list of author affiliations is available in the full article online.
*These authors contributed equally to this work.
†Corresponding author. Email: sternsons@janelia.hhmi.org
Cite this article as C. J. Magnus *et al.*, *Science* **364**, eaav5282 (2019). DOI: 10.1126/science.aav5282

RESEARCH ARTICLE

NEUROSCIENCE

Ultrapotent chemogenetics for research and potential clinical applications

Christopher J. Magnus[1]*, Peter H. Lee[1]*, Jordi Bonaventura[2], Roland Zemla[3,4], Juan L. Gomez[2], Melissa H. Ramirez[1], Xing Hu[5], Adriana Galvan[5], Jayeeta Basu[3,6], Michael Michaelides[2,7], Scott M. Sternson[1]†

Chemogenetics enables noninvasive chemical control over cell populations in behaving animals. However, existing small-molecule agonists show insufficient potency or selectivity. There is also a need for chemogenetic systems compatible with both research and human therapeutic applications. We developed a new ion channel–based platform for cell activation and silencing that is controlled by low doses of the smoking cessation drug varenicline. We then synthesized subnanomolar-potency agonists, called uPSEMs, with high selectivity for the chemogenetic receptors. uPSEMs and their receptors were characterized in brains of mice and a rhesus monkey by in vivo electrophysiology, calcium imaging, positron emission tomography, behavioral efficacy testing, and receptor counterscreening. This platform of receptors and selective ultrapotent agonists enables potential research and clinical applications of chemogenetics.

Chemogenetics (*1*) targets an exogenous receptor to a specific cell population to control cellular activity only when engaged by a selective agonist. The approach is generalizable because the same receptor and agonist combination is used for different cell types. Chemogenetic tools have widespread utility in animal models (*2*) and for therapeutic applications (*3*, *4*). However, there are fundamental shortcomings of the small-molecule agonists for research purposes (*5*–*7*). Moreover, human therapies would be facilitated by chemogenetic receptors that are potently activated by existing clinically approved drugs.

Chemogenetic systems (table S1) based on engineered G protein–coupled receptors (GPCRs) called DREADDs have been used with the agonist clozapine-*N*-oxide (CNO) (*8*, *9*), but CNO is a substrate for the P-glycoprotein efflux pump (PgP) and is metabolically converted to clozapine, which is the active agent in the brain (*5*, *6*, *10*). Clozapine binds with high affinity to many receptors and has side effects such as behavioral inhibition (*7*) and potentially fatal agranulocytosis (*11*). Chemogenetic GPCR tools often rely on GPCR overexpression (*12*) to achieve high-potency responses, and effects on cell electrical activity are variable as a result of indirect coupling to ion channels. Engineered ligand-gated ion channels (LGICs) enable direct control over cellular activity by a small molecule. However, despite decades of development, chemogenetic tools have been hindered by limitations of the small-molecule agonists.

Pharmacologically selective actuator modules (PSAMs) are a modular chemogenetic platform based on modified α7 nicotinic acetylcholine receptor (nAChR) ligand-binding domains that are engineered to selectively interact with brain-penetrating synthetic agonists called pharmacologically selective effector molecules (PSEMs). PSAMs can be combined with various ion pore domains (IPDs) from different ion channels, such as serotonin receptor 3 (5HT3) or glycine receptor (GlyR), to produce chimeric LGICs with common pharmacology but distinct functional properties (Fig. 1A). PSAM-5HT3 chimeric channels are cation-selective and PSAM-GlyR channels are chloride-selective, leading to neuron activation or silencing, respectively, in response to PSEM agonists (Fig. 1A) (*13*). Engineered chimeric channels have been used to investigate the involvement of specific neuron populations in multiple functions (*2*). The primary limitations of PSEMs are short clearance times (30 to 60 min) and low-micromolar potency (*13*), which are not ideal for in vivo applications. In addition, the sensitivity of PSAMs to clinically approved drugs is unknown. We combined structure-guided ion channel engineering with synthetic chemistry and testing by in vivo imaging, electrophysiology, and behavioral perturbation to develop an ultrapotent chemogenetic system for research and potential clinical applications.

Engineering channel sensitivity to clinically used drugs

We examined 44 clinically used drugs with chemical similarity to nicotinic receptor agonists in a membrane potential screen against a panel of 41 chimeric channels with mutant α7 nAChR ligand-binding domains spliced onto the 5HT3 IPD (α7-5HT3) (*13*) (Fig. 1B). The membrane potential assay yields dose responses that reflect sustained channel activation, which is most relevant for chemogenetic applications (fig. S1) (*13*).

The anti-emetic drug granisetron (Fig. 1C), which has no agonist activity at α7 nAChR, activated $\alpha7^{W77F}$-5HT3 [membrane potential median effective concentration ($EC50_{MP}$) = 1.2 μM] and $\alpha7^{W77Y}$-5HT3 ($EC50_{MP}$ = 1.1 μM) as well as the $\alpha7^{W77F}$-GlyR chloride-selective chimeric channel ($EC50_{MP}$ = 0.60 ± 0.07 μM; mean ± SEM) (Fig. 1D). Thus, Trp^{77} in the ligand-binding domain controls off-target selectivity of granisetron at α7 nAChR.

Another anti-emetic drug, tropisetron, and the smoking cessation drug varenicline activated many of the mutant channels (Fig. 1, B and C, and fig. S2, A and B), consistent with the established α7 nAChR agonist activity of these molecules (*14*, *15*). Mutation at Gln^{79} → Gly (Q79G) enhanced the activity of tropisetron by a factor of 4 ($EC50_{MP}$ = 38 ± 3 nM) (Fig. 1E) as well as the potency of additional α7 nAChR agonists (fig. S2). Varenicline agonist activity was slightly improved relative to α7-5HT3 with mutations at Gln^{79} → Ser ($EC50_{MP}$ = 470 ± 70 nM) or Gln^{139} → Leu ($EC50_{MP}$ = 300 nM) (fig. S2B).

Ultrapotent chemogenetic receptor for varenicline

Varenicline is an especially attractive molecule for chemogenetic applications in the central nervous system because (i) it is well-tolerated by patients at low doses (*16*, *17*), (ii) it has excellent brain penetrance (*18*), (iii) it is not a PgP substrate (*19*), (iv) it has low binding to plasma proteins, and (v) it has long-lived pharmacology in monkeys and humans (half-life $t_{1/2}$ >17 hours) and acceptable half-life in mice and rats ($t_{1/2}$ = 1.4 hours and 4 hours, respectively) (*20*). Anti-smoking activity is reportedly due to α4β2 nAChR partial agonism, but varenicline has off-target agonist activity at 5HT3-R (*21*) and at α7 nAChR (*15*), and it is the latter activity that we exploited for chemogenetic applications. Comparison of crystal structures of ACh-binding proteins complexed with varenicline or tropisetron showed distinct binding poses of the two molecules (Fig. 2A) (*22*, *23*). The tropisetron indole substituent is positioned at the binding pocket entrance, near Gln^{79}, consistent with the potency-enhancing effect of mutating Gln^{79} to smaller amino acid residues for tropisetron and other tropane and quinuclidine α7 nAChR agonists (fig. S2, C and D). In contrast, varenicline binds in an orientation

[1]Janelia Research Campus, Howard Hughes Medical Institute, Ashburn, VA 20147, USA. [2]Biobehavioral Imaging and Molecular Neuropsychopharmacology Unit, National Institute on Drug Abuse Intramural Research Program, Baltimore, MD 21224, USA. [3]Neuroscience Institute, New York University, New York, NY 10016, USA. [4]Medical Scientist Training Program, New York University School of Medicine, New York, NY 10016, USA. [5]Yerkes National Primate Research Center and Department of Neurology, Emory University, Atlanta, GA 30329, USA. [6]Department of Neuroscience and Physiology, New York University Langone Medical Center, New York, NY 10016, USA. [7]Department of Psychiatry & Behavioral Sciences, Johns Hopkins University School of Medicine, Baltimore, MD 21205, USA.
*These authors contributed equally to this work.
†Corresponding author. Email: sternsons@janelia.hhmi.org

that directs its quinoxaline ring system toward the interior of the ligand-binding domain, near Val^{106}, which is equivalent to amino acid Leu^{131} in the α7 nAChR ligand-binding domain (Fig. 2A), and this binding pose may explain the limited potency enhancement of varenicline observed for our initial panel of 41 mutant channels (fig. S2B). This amino acid residue had not been investigated previously, so we examined the influence of mutations at Leu^{131} on agonist potency.

Replacement of Leu^{131} with smaller amino acid residues markedly increased the potency of varenicline, tropisetron, and several other synthetic agonists while reducing the potency of the canonical agonists ACh and nicotine (Fig. 2B and fig. S3A). $\alpha7^{L131G}$-GlyR showed a factor of 17 potency enhancement for varenicline ($EC50_{MP}$ = 37 ± 26 nM) but only a factor of 3 improvement for tropisetron (Fig. 2B), which is consistent with their orthogonal binding orientations (Fig. 2A). On the basis of secondary screening results (fig. S2B), we combined additional mutations with $Leu^{131} \rightarrow$ Gly to further improve varenicline potency. In most cases, better varenicline potency was accompanied by an unwanted increase in ACh sensitivity (fig. S3, B and C). Nonetheless, for varenicline but not for tropisetron, some combinations were selective for agonist type: $Gln^{139} \rightarrow$ Leu and $Tyr^{217} \rightarrow$ Phe reduced ACh potency and enhanced varenicline potency (fig. S3D). The triple mutant $\alpha7^{L131G,Q139L,Y217F}$-GlyR markedly improved varenicline potency ($EC50_{MP}$ = 1.6 ± 0.1 nM), which is more potent than at the parent α7-GlyR channel by a factor of 390 (Fig. 2C). Competition binding by displacement of the selective α7 nAChR antagonist [^{3}H]-ASEM (*24*) with varenicline showed inhibitory binding constant K_i = 1.3 ± 0.4 nM at $\alpha7^{L131G,Q139L,Y217F}$-GlyR (fig. S4A), which is lower than the reported K_i of varenicline at α7 nAChR by a factor of 475 (*25*). In electrophysiological recordings from human embryonic kidney (HEK)–293 cells expressing $\alpha7^{L131G,Q139L,Y217F}$-GlyR, varenicline was a strong agonist (fig. S4, B and C, I_{VAR}/I_{ACh} = 1.9 ± 0.2, n = 13) that produced a slowly activating response, with a sustained window current balancing channel activation and inactivation, as well as a slow ligand off-rate due to the high-affinity interaction (Fig. 2D and fig. S4D). Similar response properties were also observed in an immune cell line (fig. S4, E and F), demonstrating that channel function is comparable in another cell type. The agonist selectivity of varenicline at $\alpha7^{L131G,Q139L,Y217F}$-GlyR over the drug's clinical target, α4β2 nAChR, was greater by a factor of 160 (fig. S4G), and it was more potent than at 5HT3-R by a factor of 880 (fig. S4H), indicating a good window for selective chemogenetic agonism with this drug.

The ACh potency of the $\alpha7^{L131G,Q139L,Y217F}$-GlyR chimeric channel was also reduced by a factor of 13 ($EC50_{MP}$ = 83 ± 20 μM), which is higher than basal mouse brain ACh levels (0.9 nM) by nearly five orders of magnitude (*26*). This is higher than measurements of transient ACh rises in the brain, which reach 1 to 2 μM (*27*) and do not activate the channel (fig. S4, I and J). The remarkably slow activation of α7-GlyR chimeric channels (*28*) (fig. S4I) serves as a temporal filter for fast ACh transients. Choline responsiveness was also low ($EC50_{MP}$ = 128 ± 32 μM) (fig. S4, K to M), requiring concentrations substantially higher than brain or circulating plasma levels (0.54 to 7.8 μM) (*29*, *30*).

The agonist potency of $\alpha7^{L131G,Q139L,Y217F}$-GlyR was enhanced for only a subset of α7 nAChR agonists but was reduced for others (Fig. 2B), indicating that the ligand-binding domain modifications are selective for particular chemical structures, instead of displaying a nonspecific reduction in channel activation energy. Blocking $\alpha7^{L131G,Q139L,Y217F}$-GlyR with the noncompetitive ion pore antagonist picrotoxin (PTX) did not affect the voltage clamp holding current (fig. S5A), demonstrating the absence of ligand-independent leak conductance (fig. S5B). This contrasts with other channel variants that we made based on different designs that showed enhanced potency but also constitutive conductance (fig. S6). In addition, $\alpha7^{L131G,Q139L,Y217F}$-GlyR did not respond to glycine, nor did it inhibit endogenous glycine-gated GlyR currents (fig. S5, C to E). Because of its high potency, selectivity, and lack of constitutive activity, the $\alpha7^{L131G,Q139L,Y217F}$ ligand-binding domain was selected as a chemogenetic tool that is activated by varenicline and is named PSAM^4.

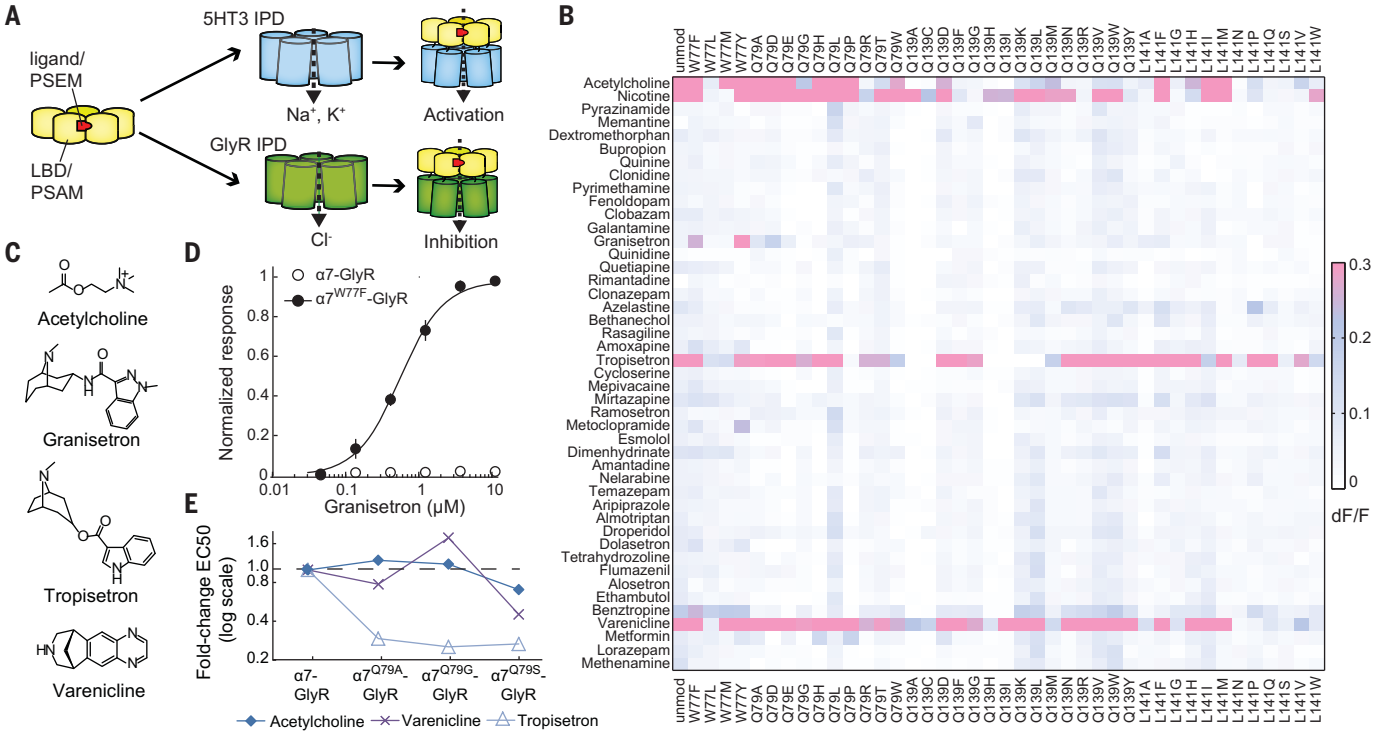

Fig. 1. Screen of mutant α7 nAChR ligand-binding domain ion channel activity against clinically used drugs. (**A**) Schematic of modular PSAM-IPD chimeric channels for cell activation and inhibition. (**B**) Screen of 41 α7-5HT3 channels with mutant ligand-binding domains against 44 clinically used drugs. (**C**) Key molecules. (**D**) Granisetron sensitivity conferred by $Trp^{77} \rightarrow$ Phe (W77F) mutation. (**E**) Tropisetron potency improved by Gln^{79} (Q79) mutations.

Neuron silencing and activation ex vivo

To test PSAM^4-GlyR as a neuronal silencer, we used in utero electroporation in mice to co-express the chemogenetic channel and enhanced green fluorescent protein (EGFP) in layer 2/3 cortical neurons (Fig. 2E). PSAM^4-GlyR–expressing neuron properties in acute brain slices were similar to those of nearby untransfected control cells (fig. S4M). Varenicline (10 to 16 nM) strongly suppressed firing (Fig. 2F) as a result of electrical shunting that, on average, reduced the input resistance by a factor of 3 (Fig. 2G) and increased the current amplitude required to fire an action potential by a factor of 6 (rheobase) (Fig. 2H), with multiple neurons not firing even with 500 pA depolarizing current. Silencing was reversible upon ligand washout, although not all cells fully recovered during the recording because of the slow off-rate of varenicline from PSAM^4-GlyR (Fig. 2D). We examined the durability of continuous silencing in cultured hippocampal neurons expressing PSAM^4-GlyR under constant exposure to 15 nM varenicline for 3 to 18 days, which maintained elevated rheobase that reversed on washout and could be resilenced by reapplication of varenicline (fig. S5, F to I). These low concentrations of varenicline for silencing are less than the estimated range of steady-state brain concentrations of varenicline in humans from a twice-daily 1-mg dose by a factor of 2 to 13 (*18*). This raises the possibility that varenicline can be used for chemogenetic applications at doses below those that are effective for anti-nicotine therapy.

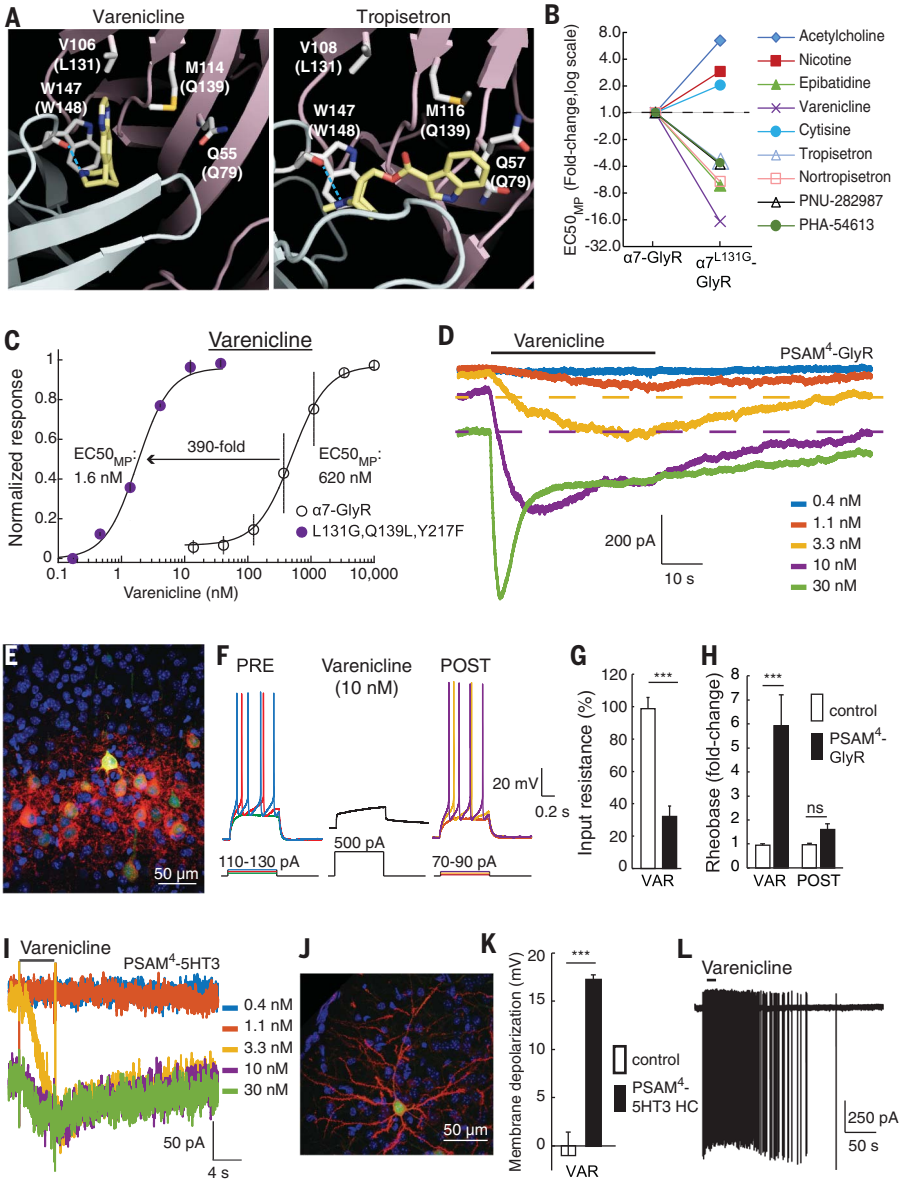

Fig. 2. Development of an ultrapotent PSAM for varenicline. (**A**) Varenicline (left) and tropisetron (right) bind ACh-binding proteins in distinct orientations. Dashed line denotes H bond with Trp^{147}; homologous α7 nAChR pre-protein numbering is in parentheses. L, Leu; M, Met; Q, Gln; V, Val; W, Trp. (**B**) Leu^{131} → Gly oppositely affects potency for varenicline, ACh, and other α7 nAChR agonists. (**C**) Potency enhancement of varenicline for α7^{L131G,Q139L,Y217F}-GlyR. (**D**) Varenicline whole-cell voltage clamp response at α7^{L131G,Q139L,Y217F}-GlyR. Baseline shifts reflect slow washout (dashed lines). (**E**) Cortical layer 2/3 neurons expressing EGFP and PSAM^4-GlyR with nonpermeabilized cell surface labeling by α-bungarotoxin–Alexa594 (αBgt-594). (**F** to **H**) Action potential firing was strongly suppressed by varenicline in neurons expressing PSAM^4-GlyR (F) as a result of reduced input resistance (G) and elevated rheobase (H). (**I**) Varenicline binding to PSAM^4-5HT3 elicits a weakly desensitizing current with high potency. Baseline shifts reflect slow washout. (**J**) αBgt-594 labeling of PSAM^4-5HT3 HC (red) on cell surface of a cortical layer 2/3 neuron coexpressing EGFP. (**K** and **L**) Varenicline (15 nM) depolarizes (K) and elicits action potentials (L) in neurons expressing PSAM^4-5HT3 HC. Error bars are SEM. ***P < 0.001 (Mann-Whitney U test); n.s., not significant (P > 0.05).

Chemogenetic silencing in mice and monkey

In vivo chemogenetic efficacy was tested with PSAM^4-GlyR in mice by targeting *Slc32a1* (*vesicular GABA transporter*)-expressing GABAergic neurons in the substantia nigra reticulata (SNr) (Fig. 3A). Unilateral silencing of SNr neurons by intracranial microinjection of the GABA receptor agonist muscimol results in rotation contraversive to the inhibited side (*31*). For chemogenetic silencing, the SNr was transduced with PSAM^4-GlyR by injection of recombinant adeno-associated virus *rAAV1-Syn::FLEX-rev-PSAM^4-GlyR–IRES–EGFP*. The dose response of varenicline-mediated PSAM^4-GlyR silencing was established by monitoring mouse rotation in the presence of low-dose amphetamine (3 mg/kg) to increase overall activity. The lowest effective dose (LED) for onset of rotation activity in PSAM^4-GlyR mice after

intraperitoneal varenicline delivery was 0.1 mg/kg (Fig. 3B and movie S1). Subsequent varenicline readministration after 5 hours reactivated rotation activity without tachyphylaxis of the chemogenetic response (Fig. 3C). Behavioral effects of silencing were evident within 20 min, and rotation activity returned nearly to baseline after 4 hours (Fig. 3D), consistent with reported varenicline half-life (*20*). These low doses of varenicline are an order of magnitude lower than those required for mice to recognize varenicline as a replacement for nicotine (*32*, *33*) or for other reported behavioral consequences in mice (*34*). In addition, oral delivery of varenicline (5 μg/ml) also elicited circling (fig. S5K).

We also tested PSAM^4-GlyR for silencing activity in a rhesus monkey in the globus pallidus internal region (GPi) (Fig. 3E). GPi was transduced with PSAM^4-GlyR by electrophysiologically guided injection of *rAAV8-Syn::PSAM^4-GlyR–IRES–EGFP* (Fig. 3, F to H). The GPi neuron firing rate and burst firing rate were significantly inhibited by subcutaneous varenicline (0.1 mg/kg) delivery relative to GPi activity in the presence of varenicline prior to AAV transduction (Fig. 3, I and J). Neither the regularity of firing (coefficient of variation for interspike interval) nor burst probability was affected by chemogenetic silencing (Fig. 3, K and L). This dose is lower than the dose required for varenicline to serve as a nicotine-substituting discriminative stimulus in monkeys by a factor of 5 (*35*).

Highly potent and selective chemogenetic agonists

Chemogenetic agonists for research applications should balance requirements for high potency, selectivity, and brain bioavailability along with pharmacodynamic responses of hours. We set out to make molecules that retained the high potency of varenicline at PSAM^4 but improved selectivity over varenicline's endogenous targets. We synthesized 30 varenicline analogs (Fig. 4A and table S2) modified at the quinoxaline portion of the molecule because of its proximity to the "hole" predicted by the Leu^{131} → Gly mutation (Fig. 2A). We chose modifications that kept structural elements and physicochemical properties within ranges associated with brain bioavailability and low PgP substrate activity (*36*). Thirteen molecules had potency below 10 nM at PSAM^4-GlyR or PSAM^4-5HT3 and had high selectivity for PSAM^4-GlyR with reduced agonist activity at the three endogenous targets of varenicline (α4β2 nAChR, α7 nAChR, and 5HT3-R) (table S2).

We focused on four molecules that had high potency in mice (Fig. 4B, table S2, and below). Quinoxalone derivative 792 (Fig. 4A, pathway e) had subnanomolar affinity for PSAM^4-GlyR (K_i = 0.7 ± 0.1 nM) (Fig. 4, C and D) and was an ultrapotent PSEM (uPSEM) agonist for PSAM^4-GlyR and PSAM^4-5HT3 (Fig. 4, B and E, and fig. S8, A and B). uPSEM^{792} showed agonist selectivity for PSAM^4-GlyR and PSAM^4-5HT3 relative to α7-GlyR, α7-5HT3, and 5HT3-R by more than four orders of magnitude (Fig. 4, B and E, and fig. S8C). At α4β2 nAChRs, uPSEM^{792} was a very weak partial agonist (10 ± 0.4%) (figs. S8D and S9A) with selectivity for PSAM^4-GlyR by a factor of 230 (Fig. 4, B and E). Thus, uPSEM^{792} retained the potency of varenicline for PSAM^4-GlyR with enhanced chemogenetic selectivity.

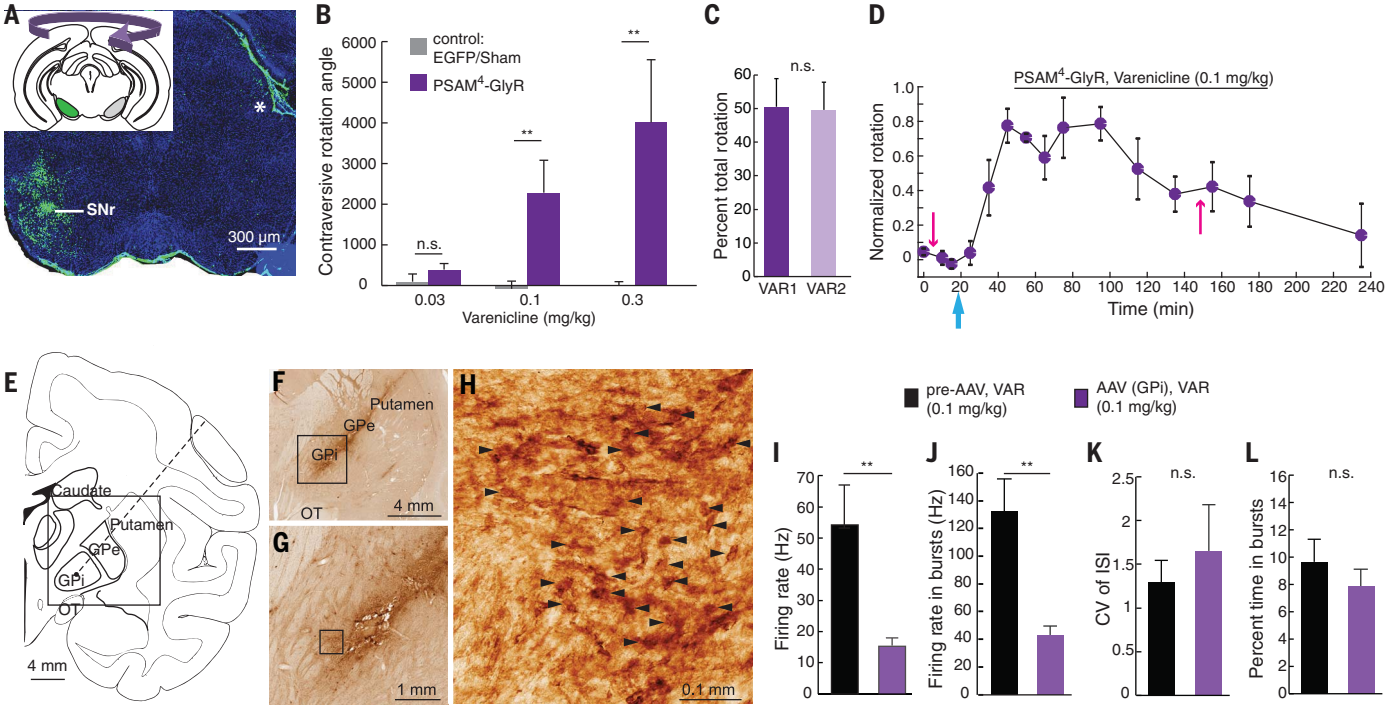

Fig. 3. PSAM^4-GlyR neuron silencing in mice and a monkey. (**A**) PSAM^4-GlyR–IRES–EGFP targeted unilaterally to the SNr. Inset: Schematic of unilateral SNr transduction and contralateral rotation. Asterisk denotes nonspecific immunofluorescence. (**B**) Low doses of intraperitoneal varenicline elicit contraversive rotation for mice expressing PSAM^4-GlyR (n = 9 mice) but not mice that were sham-operated or expressed EGFP alone (n = 6 mice). (**C**) Two doses of varenicline separated by 5 hours gave similar proportions of total rotation (n = 4 mice). (**D**) Time course of rotation response normalized to maximum rotation for each mouse (n = 4 mice). Magenta arrows, amphetamine injections; cyan arrow, varenicline injection. (**E**) Coronal diagram of rhesus macaque brain showing location of GPi targeted for AAV injection and in vivo electrophysiological recordings along trajectory shown by dashed line. Box denotes area of interest for (F). OT, optic tract; GPe, external globus pallidus. (**F** to **H**) EGFP marker gene expression near injection site. Boxes denote area of interest for subsequent panel; arrowheads (H) indicate EGFP-positive neuronal profiles visualized by 3,3′-diaminobenzidine polymerization. (**I** to **L**) In one monkey, electrophysiological reduction of overall neuronal firing rate (I) and burst firing rate (J) in GPi after peripheral varenicline injection. Coefficient of variation of interspike interval (CV of ISI) (K) and percent time in burst firing (L) were not affected (pre-AAV, n = 8 neurons; post-PSAM^4-GlyR AAV, n = 10 neurons). Error bars are SEM. **P < 0.01 (Mann-Whitney U test).

Alkoxy substitution of varenicline (Fig. 4A, pathway d) resulted in subnanomolar PSAM^4-GlyR and PSAM^4-5HT3 affinities and potencies (Fig. 4B and fig. S8, E, G, and I). The highest-affinity PSAM^4-GlyR agonist, uPSEM^{817} (K_i = 0.15 ± 0.02 nM) (Fig. 4C), was generated by propoxy substitution of varenicline and had remarkable potency ($EC50_{MP}$ = 0.3 ± 0.4 nM), which makes uPSEM^{817} one of the most potent LGIC agonists ever reported. uPSEM^{817} agonist selectivity was also excellent, with selectivity for PSAM^4-GlyR over α7-GlyR, α7-5HT3, and 5HT3-R by factors of 5000 to 10,000 (Fig. 4B). uPSEM^{815} and uPSEM^{817} did not show evident α4β2 nAChR agonism up to 30 μM (fig. S9B), and uPSEMs 793 and 815 had selectivity for PSAM^4-GlyR over 5HT3-R by a factor of >2000 (Fig. 4B and fig. S8, F and H). α7 nAChR agonism was not detected for any of the uPSEMs at 1000 times their PSAM^4-GlyR EC50 values (fig. S9, C and D).

To test for binding to a larger range of molecular targets, we used radioligand displacement against functionally important endogenous receptors and transporters (*37*). This showed no significant binding at 30 to 100 times the PSAM^4-GlyR EC50 values of the uPSEMs at 48 of 52 targets, including serotonin, GABA, adrenergic, muscarinic, dopamine, and histamine receptors (tables S3 and S4). [^{3}H]-ASEM radioligand displacement from rat forebrain tissue α7 nAChRs by uPSEMs showed high K_i values of 0.3 to 8 μM (fig. S9E). The molecules retained binding to β2-containing nAChRs, with highest affinity for α4β2 nAChR (fig. S9E and tables S3 and S4). However, for uPSEM^{792}, functional measurements of α4β2 channel activation by 1 μM ACh (a low but physiologically relevant concentration) did not show inhibitory consequences of uPSEM^{792} before the higher concentrations at which uPSEM^{792} elicited weak α4β2 agonist activity (fig. S9A), and the IC50 for uPSEM^{817} at α4β2 nAChRs was higher than its EC50 for PSAM^4-GlyR by two orders of magnitude (Fig. 4, B and F).

uPSEMs 792, 793, 815, and 817 strongly suppressed layer 2/3 cortical neurons expressing PSAM^4-GlyR in brain slices at low concentrations ranging from 1 to 15 nM (Fig. 4G and fig. S9, G to K). In addition, all uPSEMs were soluble in water. We tested the most selective uPSEMs 792 and 817 for P-glycoprotein pump efflux. They were not PgP substrates (efflux ratio < 2; Fig. 4I and table S5), indicating that they are suitable candidates for in vivo applications in the brain.

Imaging chemogenetic receptors in vivo

Delivery of chemogenetic receptors to the brain can be variable; thus, it is desirable to noninvasively monitor chemogenetic receptor expression and anatomical distribution in the brain. To noninvasively measure the distribution of PSAM^4-GlyR in vivo as well as accessibility and binding of uPSEMs in the mouse brain, we used positron emission tomography (PET). PSAM^4-GlyR expressed unilaterally in the cortex potently bound the radiolabeled α7 nAChR antagonist [^{18}F]-ASEM (*38*) at this location in vivo (Fig. 4, J and K). Receptor localization could be readily visualized against endogenous ligand binding, even with extremely low doses of the tracer. The distribution of PSAM^4-GlyR can thus be determined noninvasively with a PET ligand that has been used in humans and is suitable for both research and clinical applications.

To establish uPSEM binding to PSAM^4-GlyR in brain tissue, we used radioligand displacement. PSAM^4-GlyR–IRES–EGFP was expressed in the left dorsal striatum and EGFP alone was expressed in the right striatum. We performed autoradiography with [^{3}H]-ASEM bound to PSAM^4-GlyR in striatal brain slices to confirm ligand displacement ex vivo (fig. S9, M to O), and the radioactivity corresponded to the location of PSAM^4-GlyR–IRES–EGFP expression (fig. S9P). Next, we established brain penetrance and receptor binding of uPSEMs in vivo using PET by competition of [^{18}F]-ASEM binding with intraperitoneal (i.p.) injection of uPSEM agonists (Fig. 4L). [^{18}F]-ASEM binding in the left dorsal striatum (Fig. 4M) was eliminated by injection of these agonists (Fig. 4N). The in vivo [^{18}F]-ASEM localization matched ex vivo expression of PSAM^4-GlyR–IRES–EGFP established by post hoc fluorescence microscopy (Fig. 4O) as well as [^{3}H]-ASEM autoradiography (Fig. 4P) in the same tissue sections, but binding was not observed in the right striatum, which expressed EGFP alone.

Potent uPSEM neuron silencing in vivo

To directly monitor uPSEM^{792}-mediated neuronal silencing in vivo, we recorded calcium dynamics of hippocampal neurons in area CA1 by two-photon imaging in head-fixed mice running on a treadmill marked with texture cues (Fig. 5A). In a *Thy1::GCaMP6f* transgenic mouse, PSAM^4-GlyR was expressed in hippocampal pyramidal cells by injection of *rAAV1-CamkII::PSAM^4-GlyR–IRES–EGFP* (Fig. 5A). The field of view contained distinct domains of neurons densely and sparsely transduced with PSAM^4-GlyR–IRES–EGFP (Fig. 5B). In stationary and running behavioral epochs, which elicit different levels of CA1 activity, both domains showed similar baseline activity, indicating that expression of PSAM^4-GlyR did not perturb basal activity (Fig. 5, C and D). After intraperitoneal injection of uPSEM^{792} (3 mg/kg), the densely transduced CA1 hippocampal domains were strongly silenced, while the sparsely transduced domain showed a modest reduction in activity (Fig. 5, C and D). In mice not expressing PSAM^4-GlyR, we found no significant difference in calcium activity of CA1 pyramidal neurons after administration of uPSEM^{792} at 3 mg/kg (P = 0.9515, n = 265 neurons, 3 mice, 93.5% of median baseline activity, signed rank test). Place cells, which fire as a result of powerful circuit and cell-autonomous conductances, were also silenced by PSAM^4-GlyR and uPSEM^{792} (Fig. 5E).

Finally, to determine dose responses for uPSEMs in vivo, we used behavioral assays by measuring contralateral rotation in mice with the unilateral SNr silencing assay. The potency in mice was exceptional for uPSEM^{793} (LED = 0.03 mg/kg) (Fig. 5, F and G), which is an improvement on first-generation PSEMs by three orders of magnitude (movie S2). One of the most selective agonists, uPSEM^{792}, was active at a LED of 1 mg/kg in vivo (Fig. 5, H and I, and movie S2). uPSEM^{817} also has a favorable selectivity profile and the same LED (0.1 mg/kg) as varenicline (fig. S10 and movie S2). These low doses reflect the most selective silencing regime for these molecules. All molecules elicited durable responses of 3 to 4 hours in mice with acute intraperitoneal dosing (Fig. 5, G and I, and fig. S10), which was comparable to varenicline. To examine potential off-target behavioral effects of uPSEMs, we monitored food intake, which is sensitive to off-target 5HT3-R activation. Food consumption was not significantly altered by uPSEMs at 3 times the lowest effective doses determined in the SNr silencing assay, although food intake was reduced with elevated varenicline doses, highlighting the superior selectivity of uPSEMs (fig. S11).

Discussion

Chemogenetics permits targeted, noninvasive, and reversible perturbations of cellular function. Here, we developed a set of modular ion channels and selective, exceptionally potent agonists that are effective in the brain for rodent and primate models. Chemogenetic agonists were derived from the clinically approved drug varenicline and required optimization to balance competing needs for potency, selectivity, brain penetrance, and response times of hours. We determined the lowest effective doses of the uPSEMs and varenicline in vivo to achieve the optimal balance of efficacy and selectivity. Note that varenicline can also be used for chemogenetics at lower concentrations than those associated with anti-nicotine clinical applications (*18*).

The effectiveness, ease of use, and targeted nature of chemogenetics have made clinical applications attractive (*3*, *4*, *39*). Chemogenetics uses a limited repertoire of drug/receptor pairs but achieves diverse therapeutic effects by targeting the receptors via gene transfer to distinct regions. This offers a model for therapy that circumvents the pharmacological complexity of protein target identification followed by drug development for each new target. Our engineered ion channel technology facilitates chemogenetic therapies because it uses a well-tolerated approved drug that can potentially be used at or below doses for which it is currently approved. Clinical applications of chemogenetics are well suited for conditions that can be ameliorated by modulating cellular activity at localized sites to which the chemogenetic receptor can be delivered in the course of standard surgical procedures, such as pharmacotherapy-refractory localized pain, focal epilepsy, and some movement disorders (*4*, *39*, *40*). Our own work has revealed chemogenetic perturbations in two nodes of the basal ganglia that are associated with invasive Parkinson's disease deep brain stimulation therapies. Additional studies will be needed to establish long-term safety and efficacy with chemogenetic receptors for therapeutic applications, but this is facilitated by the current clinical

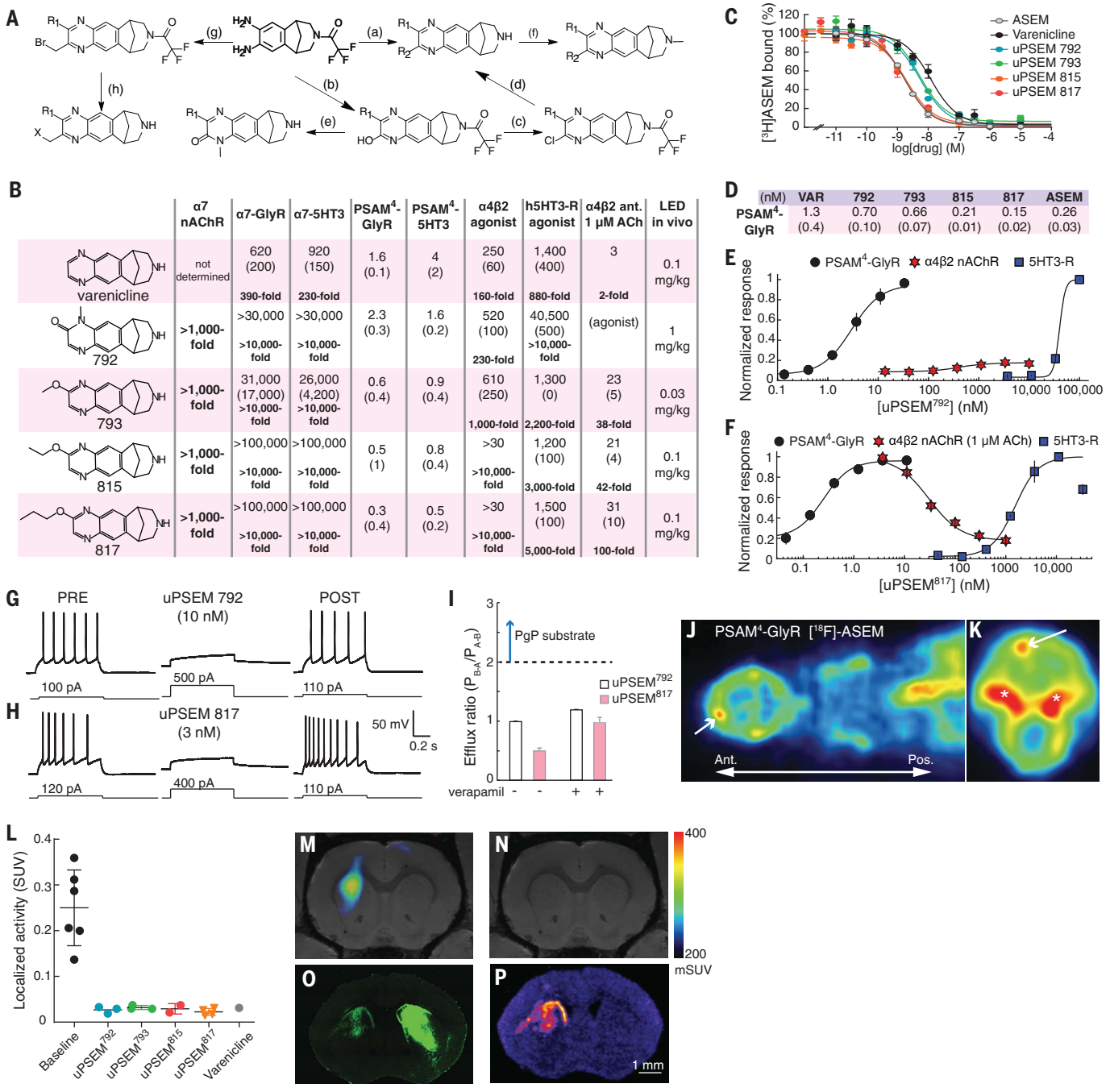

Fig. 4. Highly selective chemogenetic agonists. (**A**) Synthetic pathways (letters) for uPSEM agonists (see supplementary materials). (**B**) Comparison of uPSEM agonist EC50s at PSAM^4 channels and endogenous varenicline targets, as well as IC50 for α4β2 nAChR with 1 μM ACh. LED, lowest effective dose for mice in SNr rotation assay. Units are nM; parentheses denote SEM. Selectivity relative to PSAM^4-GlyR is shown in boldface. (**C** and **D**) Displacement of [^{3}H]-ASEM at PSAM^4-GlyR by uPSEMs (C) and K_i values (D). Parentheses denote SEM. (**E** and **F**) Dose response curves for PSAM^4-GlyR, α4β2 nAChR, and 5HT3-R. uPSEM^{792} (E) is a 10% partial agonist of α4β2 nAChR; uPSEM^{817} (F) inhibits α4β2 nAChR. (**G** and **H**) uPSEM^{792} (G) and uPSEM^{817} (H) strongly suppress firing in neurons expressing PSAM^4-GlyR. (**I**) Efflux ratio < 2, indicating that uPSEM^{792} and uPSEM^{817} are not PgP substrates. $P_{B\text{-}A}$ and $P_{A\text{-}B}$ are basal and apical permeability, respectively, across the Caco-2 cell line monolayer (n = 2 replicates). (**J** and **K**) In vivo PET imaging after [^{18}F]-ASEM injection, showing cortical localization of PSAM^4-GlyR in horizontal view through head and upper torso (J) and coronal view of the head (K). Arrow shows site of PSAM^4-GlyR expression; asterisks show accumulation of [^{18}F] outside the brain. (**L**) [^{18}F]-ASEM binding to PSAM^4-GlyR under baseline conditions and with competition by uPSEMs (uPSEM^{792}, 1 mg/kg; uPSEM^{793}, uPSEM^{815}, and uPSEM^{817}, 0.3 mg/kg) and varenicline (0.3 mg/kg). (**M**) Tomographic plane showing [^{18}F]-ASEM binding to PSAM^4-GlyR in vivo. (**N**) Competition of [^{18}F]-ASEM binding by intraperitoneally administered uPSEM^{792}. (**O** and **P**) Ex vivo fluorescence image (O) and autoradiographic image of [^{3}H]-ASEM binding (P) of corresponding brain slice expressing PSAM^4-GlyR–IRES–EGFP in left dorsal striatum. Right striatum was injected with virus expressing EGFP alone. Error bars are SEM.

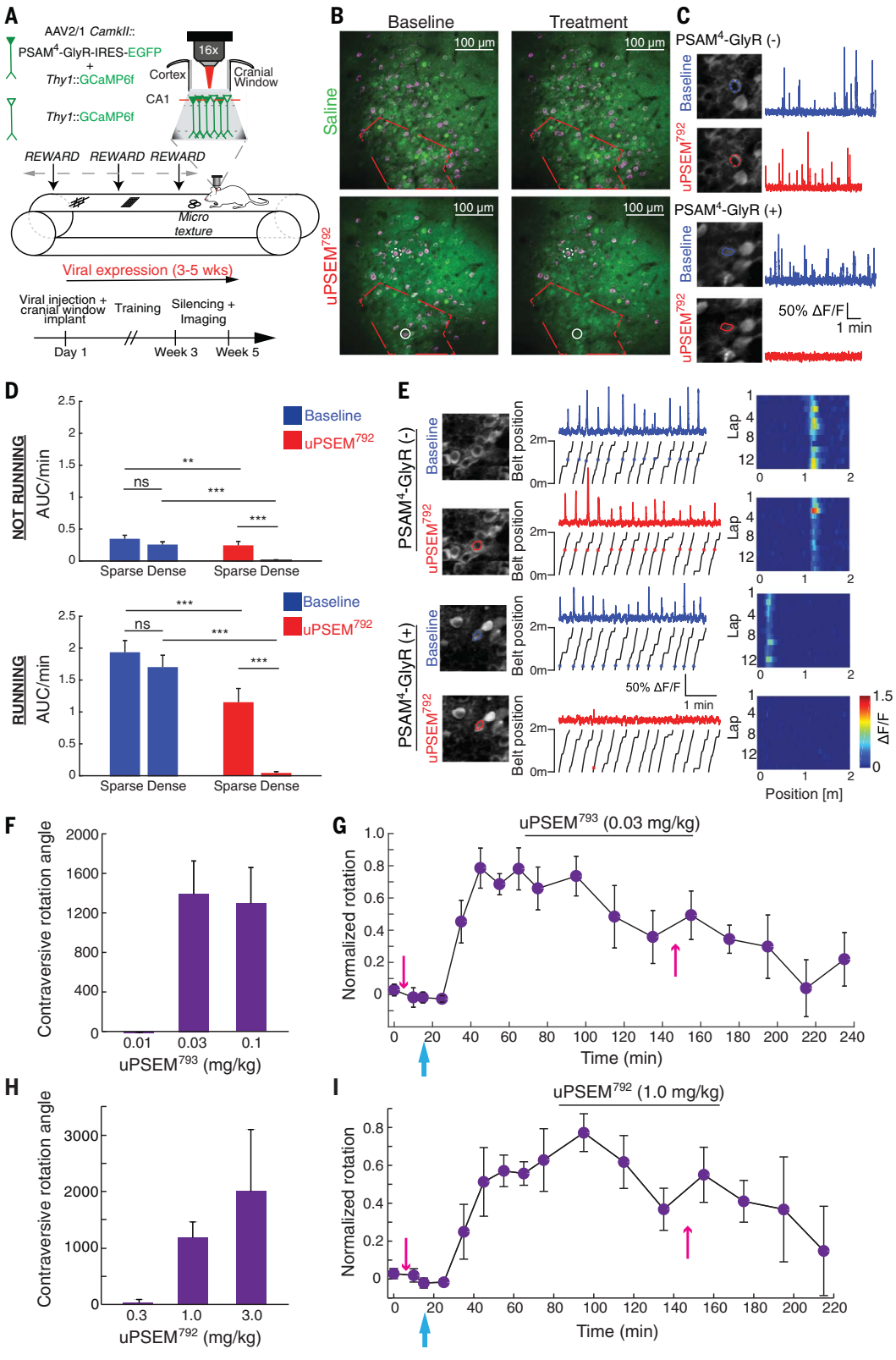

Fig. 5. Neuron silencing with uPSEMs and PSAM^4-GlyR in vivo. (**A**) Experimental design for monitoring hippocampal CA1 neuron silencing with PSAM^4-GlyR and uPSEM^{792} using in vivo two-photon Ca^{2+} imaging in head-fixed mice running on a treadmill with textural landmarks. PSAM^4-GlyR–IRES–EGFP was virally expressed in hippocampal CA1 pyramidal neurons in Thy1-GCaMP6f mice. Neurons coexpressing GCaMP6f and viral PSAM^4-GlyR–IRES–EGFP are solid green; neurons expressing only GCaMP6f are green outline. (**B**) Z-stack projections (green) overlaid with maximum-intensity projections of GCaMP6f fluorescence in time (magenta). Example images from a saline-treated (top) and uPSEM^{792}-treated (bottom) mouse. Red outline encloses densely transduced region, which also shows strong uPSEM^{792}-mediated reduction of neuron activity (reduced magenta signals). Outside the red boundary is the sparsely transduced region. Neurons depicted in (C) are circled [dashed, PSAM^4-GlyR(−); solid, PSAM^4-GlyR(+)]. (**C**) Representative regions of interest (ROIs, left) and somatic Ca^{2+} traces (right). Transduced PSAM^4-GlyR(+) pyramidal neurons are identified by EGFP-filled somata, whereas PSAM^4-GlyR(−) cells have only cytoplasmic GCaMP6f fluorescence. (**D**) Activity rate [area under $\Delta F/F$ trace of Ca^{2+} transients divided by epoch duration (AUC/min)] for episodes in which mice were running and not running on the treadmill. Densely transduced: run, n = 68 neurons, no-run, n = 58 neurons from 2 mice; sparsely transduced: run, n = 103 neurons, no-run, n = 96 neurons from 2 mice. $^{**}P < 0.01$, $^{***}P < 0.001$ (Mann-Whitney U test and signed rank test with Holm-Sidak correction). (**E**) Place field activity after uPSEM^{792} administration. Shown are somatic ROI outlines before and after treatment (left), $\Delta F/F$ activity (center top) with associated position of the mouse on the belt (center bottom), and raster plots with mean $\Delta F/F$ activity in each 2-cm spatial bin across laps (right). Asterisks denote the location of significant running calcium transients along the belt. (**F** to **I**) In vivo uPSEM dose responses for mice (n = 4) expressing PSAM^4-GlyR unilaterally in SNr. Behavioral response and time course for uPSEM^{793} [(F) and (G)] and uPSEM^{792} [(H) and (I)] are shown. Time course of rotation response is normalized to maximum rotation for each mouse. Magenta arrows, amphetamine injections; cyan arrows, uPSEM injection. Error bars are SEM.

use of varenicline. These chemogenetic technologies offer opportunities in basic research and the capability for extending findings to potential therapeutic applications.

REFERENCES AND NOTES

1. S. M. Sternson, B. L. Roth, Chemogenetic tools to interrogate brain functions. *Annu. Rev. Neurosci.* **37**, 387–407 (2014). doi: 10.1146/annurev-neuro-071013-014048; pmid: 25002280
2. D. Atasoy, S. M. Sternson, Chemogenetic Tools for Causal Cellular and Neuronal Biology. *Physiol. Rev.* **98**, 391–418 (2018). doi: 10.1152/physrev.00009.2017; pmid: 29351511
3. J. G. English, B. L. Roth, Chemogenetics—A Transformational and Translational Platform. *JAMA Neurol.* **72**, 1361–1366 (2015). doi: 10.1001/jamaneurol.2015.1921; pmid: 26409113
4. D. Kätzel, E. Nicholson, S. Schorge, M. C. Walker, D. M. Kullmann, Chemical-genetic attenuation of focal neocortical seizures. *Nat. Commun.* **5**, 3847 (2014). doi: 10.1038/ncomms4847; pmid: 24866701
5. J. L. Gomez *et al*., Chemogenetics revealed: DREADD occupancy and activation via converted clozapine. *Science* **357**, 503–507 (2017). doi: 10.1126/science.aan2475; pmid: 28774929
6. J. Raper *et al*., Metabolism and Distribution of Clozapine-N-oxide: Implications for Nonhuman Primate Chemogenetics. *ACS Chem. Neurosci.* **8**, 1570–1576 (2017). doi: 10.1021/acschemneuro.7b00079; pmid: 28324647
7. D. A. A. MacLaren *et al*., Clozapine-n-oxide administration produces behavioral effects in Long-Evans rats—implications for designing DREADD experiments. *eNeuro* **3**, 0219-16 (2016). doi: 10.1126/science.aan2475; pmid: 28774929
8. G. M. Alexander *et al*., Remote control of neuronal activity in transgenic mice expressing evolved G protein-coupled receptors. *Neuron* **63**, 27–39 (2009). doi: 10.1016/j.neuron.2009.06.014; pmid: 19607790
9. B. N. Armbruster, X. Li, M. H. Pausch, S. Herlitze, B. L. Roth, Evolving the lock to fit the key to create a family of G protein-coupled receptors potently activated by an inert ligand. *Proc. Natl. Acad. Sci. U.S.A.* **104**, 5163–5168 (2007). doi: 10.1073/pnas.0700293104; pmid: 17360345
10. M. W. Jann, Y. W. Lam, W. H. Chang, Rapid formation of clozapine in guinea-pigs and man following clozapine-N-oxide administration. *Arch. Int. Pharmacodyn. Ther.* **328**, 243–250 (1994). pmid: 7710309
11. C. J. Wenthur, C. W. Lindsley, Classics in chemical neuroscience: Clozapine. *ACS Chem. Neurosci.* **4**, 1018–1025 (2013). doi: 10.1021/cn400121z; pmid: 24047509
12. B. L. Roth, DREADDs for Neuroscientists. *Neuron* **89**, 683–694 (2016). doi: 10.1016/j.neuron.2016.01.040; pmid: 26889809
13. C. J. Magnus *et al*., Chemical and genetic engineering of selective ion channel-ligand interactions. *Science* **333**, 1292–1296 (2011). doi: 10.1126/science.1206606; pmid: 21885782
14. J. E. Macor *et al*., The 5-HT3 antagonist tropisetron (ICS 205-930) is a potent and selective α7 nicotinic receptor partial agonist. *Bioorg. Med. Chem. Lett.* **11**, 319–321 (2001). doi: 10.1016/S0960-894X(00)00670-3; pmid: 11212100
15. K. B. Mihalak, F. I. Carroll, C. W. Luetje, Varenicline is a partial agonist at α4β2 and a full agonist at α7 neuronal nicotinic receptors. *Mol. Pharmacol.* **70**, 801–805 (2006). doi: 10.1124/mol.106.025130; pmid: 16766716
16. M. Nakamura *et al*., Efficacy and tolerability of varenicline, an α4β2 nicotinic acetylcholine receptor partial agonist, in a 12-week, randomized, placebo-controlled, dose-response study with 40-week follow-up for smoking cessation in Japanese smokers. *Clin. Ther.* **29**, 1040–1056 (2007). doi: 10.1016/j.clinthera.2007.06.012; pmid: 17692720
17. K. Kaur, S. Kaushal, S. C. Chopra, Varenicline for smoking cessation: A review of the literature. *Curr. Ther. Res. Clin. Exp.* **70**, 35–54 (2009). doi: 10.1016/j.curtheres.2009.02.004; pmid: 24692831
18. H. Rollema *et al*., Pre-clinical properties of the α4β2 nicotinic acetylcholine receptor partial agonists varenicline, cytisine and dianicline translate to clinical efficacy for nicotine dependence. *Br. J. Pharmacol.* **160**, 334–345 (2010). doi: 10.1111/j.1476-5381.2010.00682.x; pmid: 20331614
19. H. M. Faessel *et al*., Lack of a pharmacokinetic interaction between a new smoking cessation therapy, varenicline, and digoxin in adult smokers. *Eur. J. Clin. Pharmacol.* **64**, 1101–1109 (2008). doi: 10.1007/s00228-008-0530-6; pmid: 18661125
20. R. S. Obach *et al*., Metabolism and disposition of varenicline, a selective α4β2 acetylcholine receptor partial agonist, in vivo and in vitro. *Drug Metab. Dispos.* **34**, 121–130 (2006). doi: 10.1124/dmd.105.006767; pmid: 16221753
21. S. C. Lummis, A. J. Thompson, M. Bencherif, H. A. Lester, Varenicline is a potent agonist of the human 5-hydroxytryptamine3 receptor. *J. Pharmacol. Exp. Ther.* **339**, 125–131 (2011). doi: 10.1124/jpet.111.185306; pmid: 21775477
22. P. Rucktooa *et al*., Structural characterization of binding mode of smoking cessation drugs to nicotinic acetylcholine receptors through study of ligand complexes with acetylcholine-binding protein. *J. Biol. Chem.* **287**, 23283–23293 (2012). doi: 10.1074/jbc.M112.360347; pmid: 22553201
23. R. E. Hibbs *et al*., Structural determinants for interaction of partial agonists with acetylcholine binding protein and neuronal α7 nicotinic acetylcholine receptor. *EMBO J.* **28**, 3040–3051 (2009). doi: 10.1038/emboj.2009.227; pmid: 19696737
24. A. G. Horti *et al*., ^{18}F-ASEM, a radiolabeled antagonist for imaging the α7-nicotinic acetylcholine receptor with PET. *J. Nucl. Med.* **55**, 672–677 (2014). doi: 10.2967/jnumed.113.132068; pmid: 24556591
25. J. W. Coe *et al*., 3,5-Bicyclic aryl piperidines: A novel class of α4β2 neuronal nicotinic receptor partial agonists for smoking cessation. *Bioorg. Med. Chem. Lett.* **15**, 4889–4897 (2005). doi: 10.1016/j.bmcl.2005.08.035; pmid: 16171993
26. P. Uutela, R. Reinilä, P. Piepponen, R. A. Ketola, R. Kostiainen, Analysis of acetylcholine and choline in microdialysis samples by liquid chromatography/tandem mass spectrometry. *Rapid Commun. Mass Spectrom.* **19**, 2950–2956 (2005). doi: 10.1002/rcm.2160; pmid: 16180202
27. V. Parikh, R. Kozak, V. Martinez, M. Sarter, Prefrontal acetylcholine release controls cue detection on multiple timescales. *Neuron* **56**, 141–154 (2007). doi: 10.1016/j.neuron.2007.08.025; pmid: 17920021
28. T. Grutter *et al*., Molecular tuning of fast gating in pentameric ligand-gated ion channels. *Proc. Natl. Acad. Sci. U.S.A.* **102**, 18207–18212 (2005). doi: 10.1073/pnas.0509024102; pmid: 16319224
29. C. A. Griffith, L. J. Owen, R. Body, G. McDowell, B. G. Keevil, Development of a method to measure plasma and whole blood choline by liquid chromatography tandem mass spectrometry. *Ann. Clin. Biochem.* **47**, 56–61 (2010). doi: 10.1258/acb.2009.008191; pmid: 19837724
30. B. Yue *et al*., Choline in whole blood and plasma: Sample preparation and stability. *Clin. Chem.* **54**, 590–593 (2008). doi: 10.1373/clinchem.2007.094201; pmid: 18310145
31. J. Scheel-Krüger, J. Arnt, G. Magelund, Behavioural stimulation induced by muscimol and other GABA agonists injected into the substantia nigra. *Neurosci. Lett.* **4**, 351–356 (1977). doi: 10.1016/0304-3940(77)90183-5; pmid: 19556189
32. C. S. Cunningham, L. R. McMahon, Multiple nicotine training doses in mice as a basis for differentiating the effects of smoking cessation aids. *Psychopharmacology* **228**, 321–333 (2013). doi: 10.1007/s00213-013-3037-5; pmid: 23494230
33. F. B. de Moura, L. R. McMahon, The contribution of α4β2 and non-α4β2 nicotinic acetylcholine receptors to the discriminative stimulus effects of nicotine and varenicline in mice. *Psychopharmacology* **234**, 781–792 (2017). doi: 10.1007/s00213-016-4514-4; pmid: 28028600
34. N. C. Ortiz, H. C. O'Neill, M. J. Marks, S. R. Grady, Varenicline blocks β2*-nAChR-mediated response and activates β4*-nAChR-mediated responses in mice in vivo. *Nicotine Tobacco Res.* **14**, 711–719 (2012). doi: 10.1124/jpet.112.193078; pmid: 22438471
35. C. S. Cunningham, M. A. Javors, L. R. McMahon, Pharmacologic characterization of a nicotine-discriminative stimulus in rhesus monkeys. *J. Pharmacol. Exp. Ther.* **341**, 840–849 (2012). doi: 10.1124/jpet.112.193078; pmid: 22438471
36. S. A. Hitchcock, Structural modifications that alter the P-glycoprotein efflux properties of compounds. *J. Med. Chem.* **55**, 4877–4895 (2012). doi: 10.1021/jm201136z; pmid: 22506484
37. J. Besnard *et al*., Automated design of ligands to polypharmacological profiles. *Nature* **492**, 215–220 (2012). doi: 10.1038/nature11691; pmid: 23235874
38. D. F. Wong *et al*., Human brain imaging of α7 nAChR with [^{18}F]ASEM: A new PET radiotracer for neuropsychiatry and determination of drug occupancy. *Mol. Imaging Biol.* **16**, 730–738 (2014). doi: 10.1124/jpet.112.193078; pmid: 22438471
39. G. A. Weir *et al*., Using an engineered glutamate-gated chloride channel to silence sensory neurons and treat neuropathic pain at the source. *Brain* **140**, 2570–2585 (2017). doi: 10.1093/brain/awx201; pmid: 28969375
40. S. Hirschberg, Y. Li, A. Randall, E. J. Kremer, A. E. Pickering, Functional dichotomy in spinal- vs prefrontal-projecting locus coeruleus modules splits descending noradrenergic analgesia from ascending aversion and anxiety in rats. *eLife* **6**, e29808 (2017). doi: 10.7554/eLife.29808; pmid: 29027903

ACKNOWLEDGMENTS

We thank J. Lindstrom for providing stable cell lines expressing human α4β2 nAChR or α7 nAChR. Receptor counter-screening and associated K_i determinations were generously provided by the National Institute of Mental Health's Psychoactive Drug Screening Program, contract HHSN-271-2013-00017-C (NIMH PDSP). We are grateful for support from Janelia core facility staff; S. Lindo performed in utero electroporations. **Funding:** Supported by HHMI (S.M.S., C.J.M., P.H.L., and M.H.R.); NIH grant ORIP OD P51-OD011132 to the Yerkes National Primate Research Center (X.H. and A.G.); the Alfred P. Sloan Foundation, Klingenstein-Simons Foundation, NIH grant NINDS 1R01 NS109362-01, and Whitehall Foundation (J.Ba.); and National Institute for Drug Abuse Intramural Research Program ZIA000069 with support via the Resource for Molecular Imaging Agents in Precision Medicine (P41EB024495) at JHU (M.M.). **Author contributions:** C.J.M. performed ex vivo electrophysiology and SNr silencing behavioral experiments; P.H.L. developed and synthesized uPSEMs and performed dose response assays with C.J.M.; M.H.R. made ion channel constructs; J.Bo., J.L.G., and M.M. performed PET imaging and radioligand displacement at PSAM^4-GlyR and α7 nAChR; X.H. and A.G. performed rhesus macaque experiments; R.Z. and J.Ba. performed in vivo calcium imaging; and S.M.S. conceived the project, designed experiments, and wrote the paper with input from all the authors. **Competing interests:** S.M.S., C.J.M., and P.H.L. have pending patents on this technology and own stock in Redpin Therapeutics Inc., which is a biotech company focusing on therapeutic applications of chemogenetics. S.M.S. is a cofounder and consultant for Redpin Therapeutics Inc. M.M. is a cofounder and owns stock in Metis Laboratories Inc. **Data and materials availability:** All data to support the conclusions of this manuscript are included in the main text and supplementary materials. Plasmids and AAV vectors are available from www.addgene.org/browse/article/28196963/. Accession numbers are PSAM^4-GlyR (MK492109), PSAM^4-5HT3 (MK492107), PSAM^4-5HT3 HC (MK492108). uPSEM^{792} and uPSEM^{817} are available from Tocris. DNA constructs and viral vectors for PSAMs and uPSEMs are available from S.M.S. under a material agreement with the Howard Hughes Medical Institute.

SUPPLEMENTARY MATERIALS

www.sciencemag.org/content/364/6436/eaav5282/suppl/DC1
Materials and Methods
Figs. S1 to S11
Tables S1 to S6
Movies S1 and S2
References (*41*–*78*)

30 September 2018; accepted 15 February 2019
Published online 14 March 2019
10.1126/science.aav5282